MODELING OF WATER INJECTION INTO A VACUUM

John W. Alred
Hernandez Engineering, Inc., Houston, TX

L. Nicole Smith and K. C. Wang
Lockheed Martin, Houston, TX

Forrest E. Lumpkin and Steven M. Fitzgerald
NASA/JSC, Houston, TX

Abstract

A loosely coupled two-phase vacuum water plume model has been developed. This model consists of a source flow model to describe the expansion of water vapor, and the Lagrangian equations of motion for particle trajectories. Gas/Particle interaction is modeled through the drag force induced by the relative velocities. Particles are assumed traveling along streamlines. The equations of motion are integrated to obtain particle velocity along the streamline. This model has been used to predict the mass flux in a 5 meter radius hemispherical domain resulting from the burst of a water jet of 1.5 mm in diameter, mass flow rate of 24.2 g/s, and stagnation pressure of 21.0 psia, which is the nominal Orbiter water dump condition. The result is compared with an empirical water plume model, deduced from a video image of the STS-29 water dump. To further improve the model, work has begun to numerically simulate the bubble formation and bursting present in a liquid stream injected into a vacuum. The technique of smoothed particle hydrodynamics was used to formulate this simulation. A status and results of the on-going effort are presented and compared to results from the literature.

Introduction

The Orbiter dumps a combination of waste and condensate water from a port-side, heated, knife-edge nozzle, approximately every 3 days. The narrow jet of water injected into vacuum quickly bursts into a disperse plume of vapor, water droplets, and ice particles. The expanding plume may make contact with surfaces, and therefore stick and leave solid contents as permanent deposits. The optical properties of the impacted surfaces may be affected to a degree that inhibits their proper function. Phenomena that occur when a liquid stream is injected into a vacuum environment have been studied by Fuchs and Legge[1] and by Muntz and Dixon[2]. In general, as a liquid stream is discharged into a vacuum, due to the sudden drop of pressure, the stream becomes superheated and vapor bubbles may form inside the stream. As the bubble continues to grow, it eventually reaches a critical size which causes the jet to burst into water droplets and ice

fragments. The fragments form a conically shaped plume. The burst distance and the characteristic cone angle are affected by the initial stream velocity, temperature and diameter. The effect of these parameters on the burst distance and the characteristic cone angle were studied. The results of these parametric studies are presented in the following section. For the purpose of predicting the extent of contamination due to the Orbiter water dump, an engineering model has been developed to model the fast expanding gas vapor and the conical cloud of ice fragments. This model consists of a source flow model to describe the vapor phase of the plume, and the Lagrangian equations of motion for particle trajectories. The interaction between the particle and gas is modeled through only the drag induced by the relative velocities[3]. Particle number density along the plume centerline was deduced from a vacuum venting test conducted at Arnold Engineering Development Center (AEDC)[4,5]. A normal distribution function is used to describe the particle number density in the polar direction. The variance of this distribution may vary and two values of distribution variance based on the plume cone half angle have been examined. Given a location with respect to the nozzle exit, this model can predict mass flux at the specified location due to the dump. This paper will provide a detailed description of the model and the numerical procedure used. This model has been used to generate the mass flux in a 5 meter radius hemispherical domain resulting from the burst of a water jet of 1.5 mm in diameter, mass flow rate of 24.2 g/s and stagnation pressure of the jet is equal to 21.0 psia, corresponding to the nominal Orbiter water dump condition. The result is compared with the result obtained from a purely empirical model, deduced from a video image of the STS-29 water dump[6]. Model improvements via a new numerical simulation will then be discussed.

Cavitation of Liquid Streams in a Vacuum

The equation of motion for the radius R_b of a bubble in a viscous liquid as a function of time is

$$R_b \ddot{R}_b + \frac{3}{2} \dot{R}_b^2 = \frac{\Delta P}{\rho_l} - \frac{2\sigma}{\rho_l R_b} - \frac{4\mu \dot{R}_b}{\rho_l R_b} \qquad (1)$$

where σ is the surface tension, ρ_l is the density of the liquid stream, and μ is the viscosity[7]. ΔP is the pressure difference driving the bubble expansion and can be expressed as

$$\Delta P = p_{vb} - \frac{\sigma}{R_0} - \frac{p_v}{2} \qquad (2)$$

where p_{vb} is the vapor pressure of the liquid at the bubble wall temperature. The vapor pressure is given by the Clausius-Clapeyron equation

$$p_v = p_R \exp\left(-\frac{m_l l_v}{kT_s}\right) \qquad (3)$$

where p_R is a constant obtained empirically, m_l is the mass of a liquid molecule, l_v is the heat of vaporization, k is the Boltzmann constant, and T_s is the surface temperature. The reduction of the surface temperature with time of a water stream due to evaporation as given in Fuchs and Legge[1] is

$$T_0 - T_s(t) = \frac{1}{\sqrt{\pi \rho c_p \alpha}} \int_0^t \frac{\dot{q}(\tau)}{\sqrt{t-\tau}} d\tau \qquad (4)$$

where α is the thermal conductivity, T_0 is the initial stream temperature, and $T_s(t)$ is the stream surface temperature at time t.. The time-dependent surface heat transfer for vaporization is

$$\dot{q}(t) = \frac{m_l n_{vs}}{4} \bullet \sqrt{\frac{8kT_s}{\pi m_l l_v}} \qquad (5)$$

where n_{vs} is the vapor number density at temperature T_s. The definite integral of equation (4) has the interesting property that it is dominated by the value of integrand near $t = \tau$.. A useful approximation, as given in Muntz and Dixon[2], which permits a simple explicit expression to be derived, is to assume that $\dot{q}$ is constant at its value at the end of the time interval. It follows that the surface temperature can then be obtained by solving the following non-linear equation

$$T_0 - T_s(t) = \frac{\sqrt{4\alpha t/\pi \rho c_p}}{\alpha} \dot{q}(t) \qquad (6)$$

where c_p is the specific heat at a constant pressure.

Equation (1) is solved by using a third order Runge-Kutta integrator[8]. At each time step, equation (6) is solved to obtain stream temperature. From Muntz and Dixon[2], in order for a vapor bubble to exist or grow, its internal pressure must be at least

$$p_b = p_s + \sigma/R_0 + 2\sigma/R_b \qquad (7)$$

where p_s is surface pressure of the jet stream, R_0 is the radius of the stream, and R_b is the radius of the bubble. If we assume there are no temperature gradients in the stream, the internal bubble pressure must be the vapor pressure and $p_s = p_v/2$, or $p_s = 0$ for a very cold surface. The bubble must have at least a radius of R_b as solved for in equation (7), if the bubble is to begin growing. The equilibrium bubble radius, or minimum radius that will permit growth is

$$R_{be} = \frac{2\sigma}{(p_v/2 - \sigma/R_0)} \qquad (8)$$

or, for a cold stream surface,

$$R_{be} = \frac{2\sigma}{(p_v - \sigma/R_0)} \qquad (9)$$

It is assumed that bursting takes place when a bubble grows to be the size of the stream, and that the perpendicular particle velocity is equal to the growth rate of the bubble, $\dot{R}_b$. Therefore, the cone half angle of the region containing majority of ice fragments is given by

$$\theta = \arctan(\dot{R}_b/V_0) \qquad (10)$$

where V_0 is the initial stream velocity. Equation (1) has been solved for a 1.5 mm stream at various temperatures and velocities. Figure 1 shows the effect of stream temperature to the bubble growth rate. The result is plotted as R_b/R_0 versus a non-dimensional time (tV_0/R_0). Note that the stream is assumed to have burst at $R_b/R_0 = 1$. From Figure 1, we can see that the burst distance decreases with increasing stream temperature. Figure 2 shows the effect of stream velocity on the burst distance. Again, the result is plotted as R_b/R_0 versus the non-dimensional time. From this figure, we can see that the burst distance increases with increasing stream velocity. Figure 3 is a composite plot of burst distance versus stream temperature at various stream velocities. Again, the decrease of burst distance with increasing temperature is clearly shown. Figure 4 is a composite plot of burst distance versus stream velocity at various stream temperatures. Figure 5 is a composite plot of burst angle versus temperature at two different velocities. From this figure we can see that the burst cone angle increases with increasing temperature, and also the cone angle decreases with increasing velocity.

Plume Flow

After bursting, the liquid stream becomes a cloud of gas, liquid droplets and ice fragments. In this work to date, we assume all liquid droplets are solidified. Therefore, only the gas phase and ice particles are being considered in this paper. However, with the SPH technique and the SPHINX model, our ultimate goal is the modeling of gas, liquid drops, and solid particles.

Gas Phase

The fast expansion of the gas phase is characterized by high Mach numbers and velocity; and, therefore, almost straight streamlines, which seem to originate at the burst point. This type of flow can be describe by a source flow model[9]. In such a flow the density at a distance r from the burst point is given by

$$\frac{\rho}{\rho_0} = \frac{A_p}{r^2}(\cos\frac{\pi}{2}\frac{\theta}{\theta_{lim}})^{2/(\gamma-1)} \qquad (11)$$

where ρ is the stagnation density, θ is the polar angle, θ_{lim} is the limiting angle of the expanding gas, and γ is the ratio of specific heats. A_p is a constant which is calculated by mass flow considerations

$$A_p = \frac{u^*/(2u_{lim})}{\int_0^{\theta_{lim}}(\cos\frac{\pi}{2}\frac{\theta}{\theta_{lim}})^{2/(\gamma-1)}\sin\theta d\theta} \qquad (12)$$

where u^* is the velocity at sonic condition. u_{lim} is the limiting velocity and is given by

$$u_{lim} = \sqrt{\frac{2\gamma}{\gamma-1}RT_0} \qquad (13)$$

where R is the specific gas constant and T_0 is the stagnation temperature. The velocity at a distance r from the burst point is computed from the isentropic expansion relation

$$u^2[\frac{1}{M^2(\gamma-1)}+\frac{1}{2}] = \frac{a_0^2}{\gamma-1} \qquad (14)$$

where a_0 is the stagnation speed of sound. The Mach number M is computed from the area Mach number relation

$$\left(\frac{A}{A^*}\right)^2 = \frac{1}{M^2}[\frac{2}{\gamma+1}(1+\frac{\gamma-1}{2}M^2)]^{(\gamma+1)/(\gamma-1)} \qquad (15)$$

The area Mach number relation is solved by using the Newton's method.

Particle Phase

The particulate model is taken from Holcomb[3], which implements a Lagrangian treatment for the particles. The particles are assumed to be solid (no mass transfer or size change) and dilute (negligible volume in comparison to the gas), but the gas/particle system is assumed to be in non-equilibrium, in that there are relative velocities between ice particles and the expanding gas. The Lagrangian treatment of the particles, also referred to as the particle trajectory model, utilizes the natural equations of motion of the individual particles.

Particle/gas momentum interaction term accounts for the acceleration which the gaseous phase imparts on the solid particles. The Lagrangian equations of motion for the particles are

$$\frac{dR_p}{dt} = u_p \qquad (16)$$

$$\frac{du_p}{dt} = \frac{D}{m}(u_g - u_p) \qquad (17)$$

where R_p and u_p are position and velocity of particle along a streamline. u_g is the velocity of the gas at the streamline location and D is a drag related term and is given by

$$D = \frac{\pi}{2}r_p^2\rho_g C_d|u_g - u_p| \qquad (18)$$

$$C_d = \frac{24}{Re_p}[1+\frac{1}{6}Re_p^{\frac{2}{3}}] \quad for\, Re_p < 1000 \qquad (19)$$

$$C_d = 0.424 \quad for\, Re_p > 1000 \qquad (20)$$

where Re_p is the Reynolds number based on the particle diameter. Equations (16) and (17) are integrated using a third-order variable step Runge-Kutta integrator. At each time step, u_g is computed from equations (14) and (15).

Initial Results and Discussion

The model described above has been coded and used to predict the mass flux in a 5 meter radius hemispherical domain, resulting from the burst of a water jet from a nominal Orbiter water dump. The diameter of the jet is 1.5 mm, the stagnation pressure is 21.0 psia and the mass flow rate equals to 24.2 g/s. A vacuum water venting experiment was conducted at the AEDC 4- by 10-ft Research Vacuum Chamber (RVC) during 1983. Average particle sizes, particle number

densities and mass fraction were either measured or deduced from test data[4,5]. It was found that particle number density varies as $1/r^2$ down the centerline of the plume. The number density in the polar direction has a bell shaped distribution from the centerline of the plume. These observations have been incorporated into the model. Two particle sizes were chosen, large particle with mean diameter of 1.0 mm and small particle with mean diameter of 0.15 μm. The mass fraction of the large particle is 0.78; the mass fraction of the small particle is 0.02; and the mass fraction of the gas is 0.20. Number density distribution of particles varies as $1/r^2$ down the plume centerline; and a normal distribution function was used to describe number density distribution in the polar direction. The value of the number density at a reference point was scaled down from the AEDC test, such that the mass flow rate is equal to 24.2 g/s. The reference point is at 1.0 cm down stream of the nozzle exit or the burst point. Standard deviation of the normal distribution function was set equal to either the bursting half angle or half of the bursting half angle. The former is designated as the 1σ case and the latter as the 2σ case. The results are then compared with the result obtained form an empirical model deduced form a video image of the STS-29 water dump[6]. Figure 6 shows the mass flux contours obtained from the empirical model. Figure 7 shows the mass flux contours obtained from the 1σ case. Figure 8 shows the comparison of mass flux at r = 5.0 m. This figure is plotted as mass flux versus polar angle, with 0 degree at the centerline of the plume. Figure 9 is an expanded view between 0 and 20 degrees of Figure 8. Figure 10 shows the mass flux contours plot of the 2σ case. Figure 11 shows the comparison of mass flux at r = 5.0 m between the 2σ case and the empirical model. Again, the figure is plotted as mass flux versus polar angle. Figure 12 is an expanded view between 0 and 20 degrees of figure 11. From these plots, we can see that fairly good comparison between the engineering model described in this document and the empirical model was obtained. The result from the empirical model falls somewhere in between the 1σ and the 2σ cases.

Model Improvements

The current model for the Orbiter water dump is based on the semi-empirical results from the literature[2,4,5]. However, a mathematical model of the liquid flow into the vapor/ice cloud is desired. In general, as a liquid stream is discharged into a vacuum, due to the sudden drop of pressure, the stream becomes superheated and vapor bubbles may form inside the stream. As a bubble continues to grow, it eventually reaches a critical size which causes the jet to burst into water droplets and ice fragments. The fragments form a conically shaped plume. The burst distance and the characteristic cone angle are affected by the initial

stream velocity, temperature and diameter. The technique of Smooth Particle Hydrodynamics (SPH) was chosen to build this model. The intent of the model improvement using SPH is to model the bubble formation and bursting

Smoothed Particle Hydrodynamics

SPH is a relatively new technique for hydrodynamic calculations. It is a gridless Lagrangian method using a pseudo-particle interpolation method to compute smooth hydrodynamic variables, thus solving the Lagrangian equations of hydrodynamics. Each pseudo-particle has a mass, Lagrangian position and velocity, and internal energy, whereas other quantities are derived by interpolation or from constitutive relations. The major advantages of SPH are its relative ease of coding and its ability to handle irregular geometries and boundary conditions. A major disadvantage to SPH is it seldom "crashes" if something unphysical is done. Hence, one must continually ascertain that physical properties are conserved or realistic. Excellent reviews of the SPH method are given in Monaghan[10,11] and Benz[12].

A copy of an SPH code named SPHINX was obtained from the Los Alamos National Laboratory (LANL). This particular code had been tested and verified on a number of projectile impacts (see Figures 13-16) and astrophysical problems[13,14]. However, the physical properties of radiative cooling, evaporative cooling, and surface tension were lacking in SPHINX. Work has been begun at JSC to implement these effects into an SPH formulation and add these models to SPHINX. Work has also been initiated at LANL to update SPHINX to make it more responsive to the Orbiter water dump problem. Unfortunately, the results of these efforts were not ready at the time of pre-conference publication. It is hoped that these results will be presented at the conference.

Conclusions

From the previous section, one can see that the result obtained from the engineering model described in this document agrees well with the empirical model deduced form the video image. The main uncertainties of the engineering model are particle sizes, and number density distribution. To improve the model, further analysis of the available test data to derive correlation between particle sizes, number density, and distribution variance, versus initial stream condition will be conducted. Theoretical modeling of the bursting phenomenon will be accomplished to further improve the model. This update will focus on the use of the SPHINX code.

References

1. Fuchs, H. and Legge H., ``Flow of a Water Jet into Vacuum," Acta Astronautica, Vol. 6, 1979, pp. 1213-1226.

2. Muntz, E. P. and Dixon, M., ``Characteristics, Control, and Uses of Liquid Streams in Space," AIAA-85-0305, Jan. 1985.

3. Holcomb, J. E., ``Generalized Implicit Flow Solver (GIFTS) Code," 19th JANNAF Exhaust Plume Technology Subcommittee Meeting, CPIA Pub. 586, pp. 241-252, May 1991.

4. Curry, B. P., Bryson, R. J., Seiber, B. L., and Jones, J. H., ``Selected Results from an Experiment Venting an H_2O Jet into a High Vacuum," AEDC-TR-84-28.

5. Curry, B. P., Bryson, R. J., Seiber, B. L., and Jones, J. H., ``Additional Results from an Experiment Venting an H_2O Jet into a High Vacuum," AEDC-TR-85-3.

6. Hakes, C. L., Rios, E. R., Warrington, D. J., Soares, C. E., and Stafford, D., "International Space Station External Contamination Assessment," JSC-27364, March 1996.

7. Van Stralen, S. and Cole, R., ``Boiling Phenomena," Edited by S. Van Stralen and R. Cole, McGraw-Hill, New York, 1979, Vol. 1, Chap. 7, p. 197.

8. Panton, R. L., ``Incompressible Flow," John Wiley & Sons, 1984.

9. Dettleff, G., ``Plume Flow and Plume Impingement in Space Technology," Prog. Aerospace Sci. Vol. 28, pp. 1-77, 1991.

10. Monaghan, J. J., "An Introduction to SPH," Comput. Phys. Comm., Vol. 48, pp. 89-96, 1988.

11. Monaghan, J. J., "Smoothed Particle Hydrodynamics," Annu. Rev. Astron. Astrophys., Vol. 30, pp. 543-574, 1992.

12. Benz, W., "Smooth Particle Hydrodynamics: A Review"; "The Numerical Modeling of Nonlinear Stellar Pulsations," J. R. Buchler (ed.), pp. 269-288, 1992.

13. Wingate, C., R. Stellingwerf, R. Davidson, and M. Burkett, "Models of High Velocity Impact Phenomena," Int. J. Impact Engng., Vol. 14, 819-830, 1992.

14. Mandell, D.,C. Wingate, and L. Schwalbe, "Simulation of a Ceramic Impact Experiment Using the SPHINX Smooth Particle Hydrodynamics Code," 16th International Symposium on Ballistics, San Francisco, CA, Sept. 23-28, 1996.
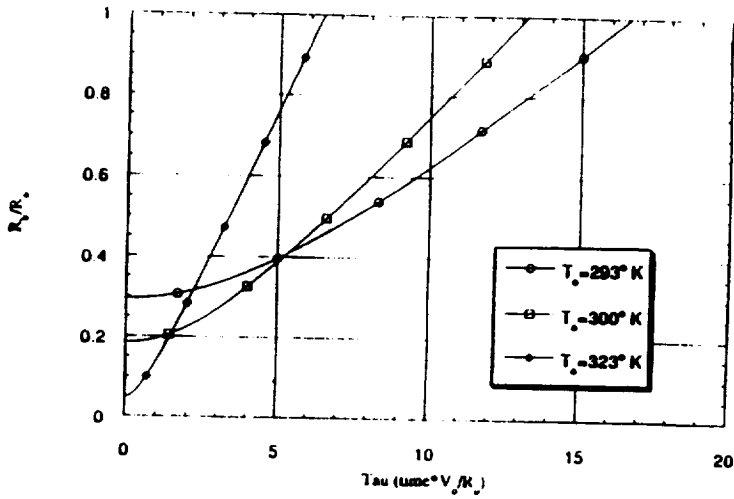
Figure 1 : Effect of Temperature on Bubble Growth
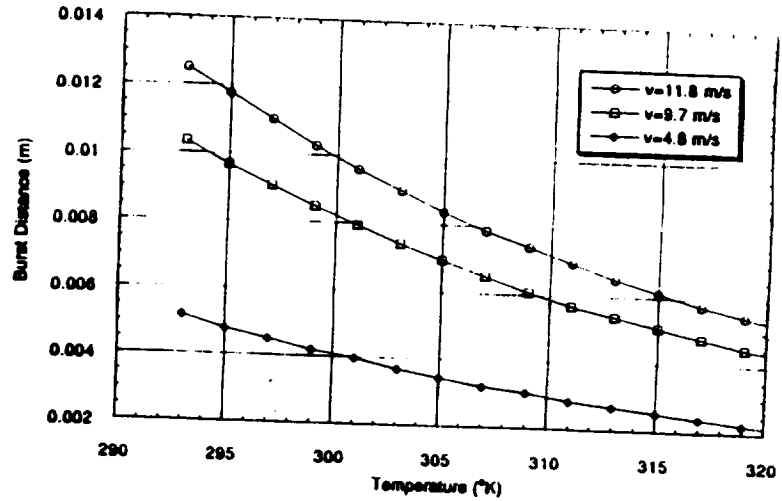
Figure 3 : Composite Plot of Burst Distance versus Stream Temperature
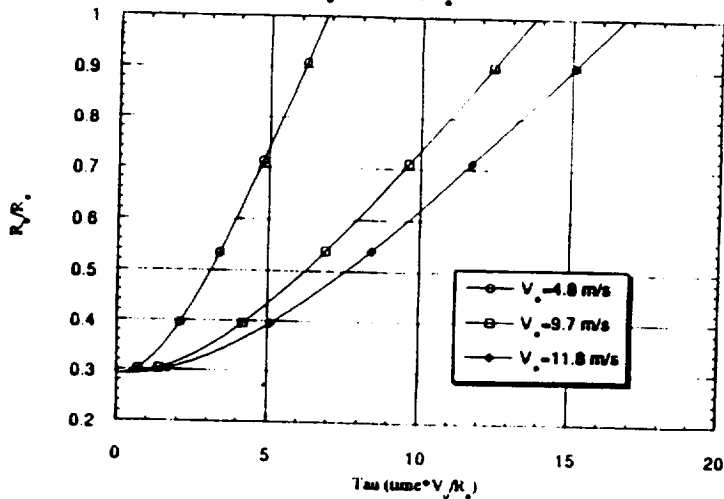
Figure 2 : Effect of Stream Velocity on Bubble Growth
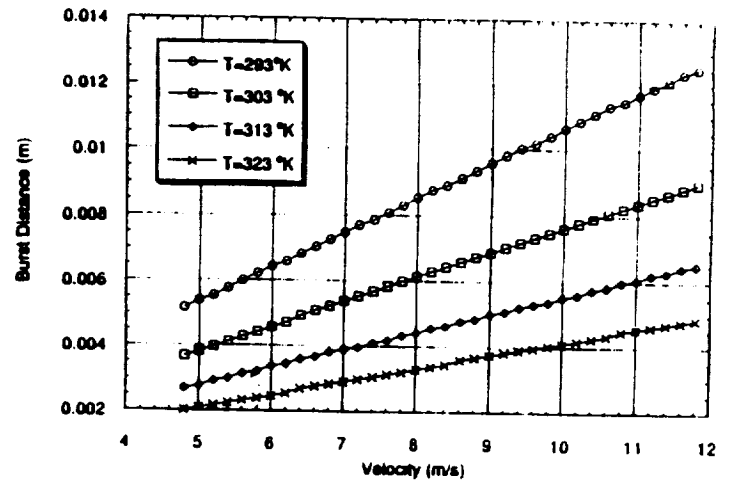

Figure 4 : Burst Distance versus Stream Velocity
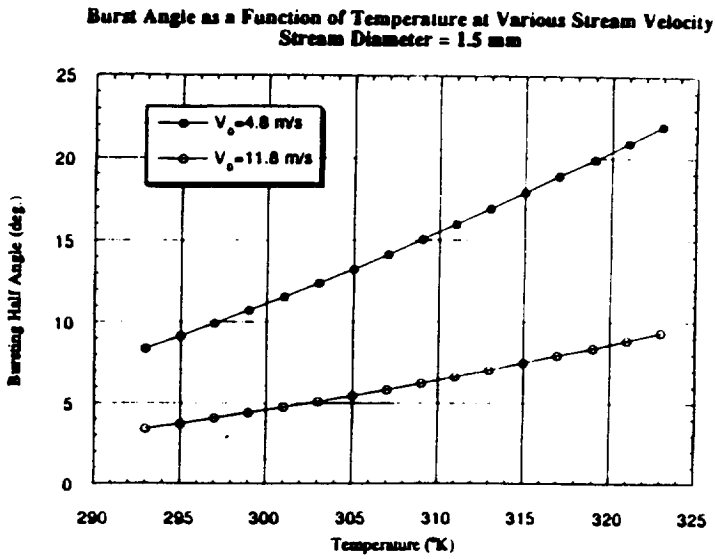
4-6

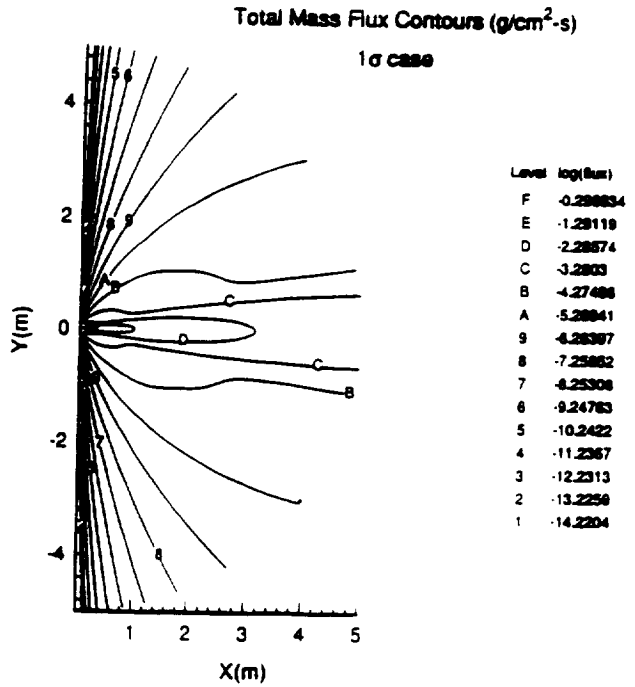Figure 5 : Composite Plot of Plume Cone Half Angle versus Stream Temperature
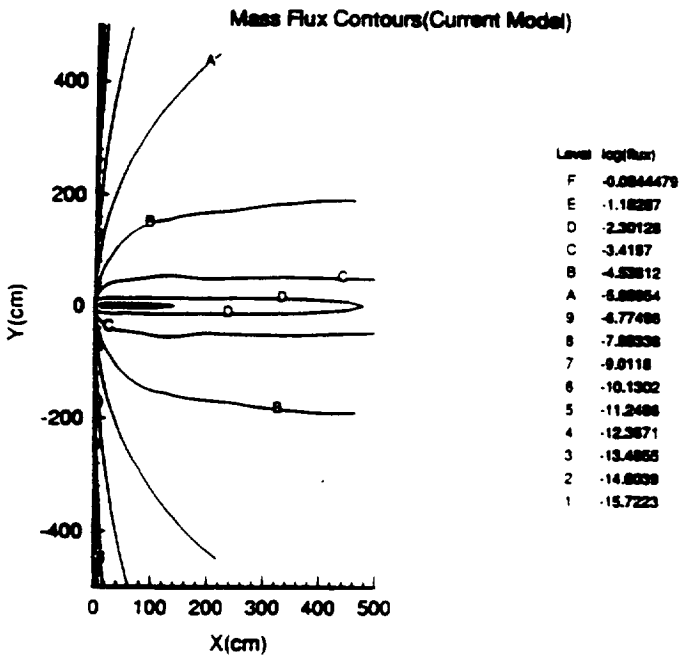

Figure 7 : Mass Flux Contours for the 1σ case
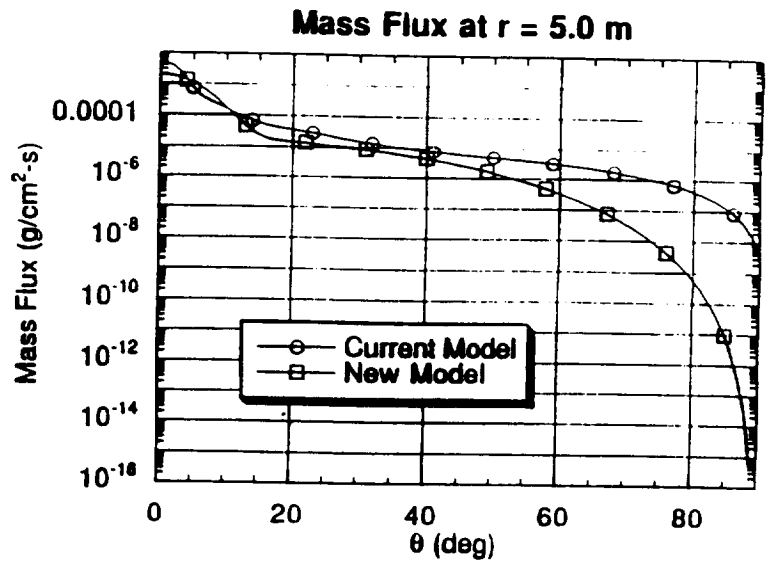

Figure 6 : Mass Flux Contours of Empirical Model

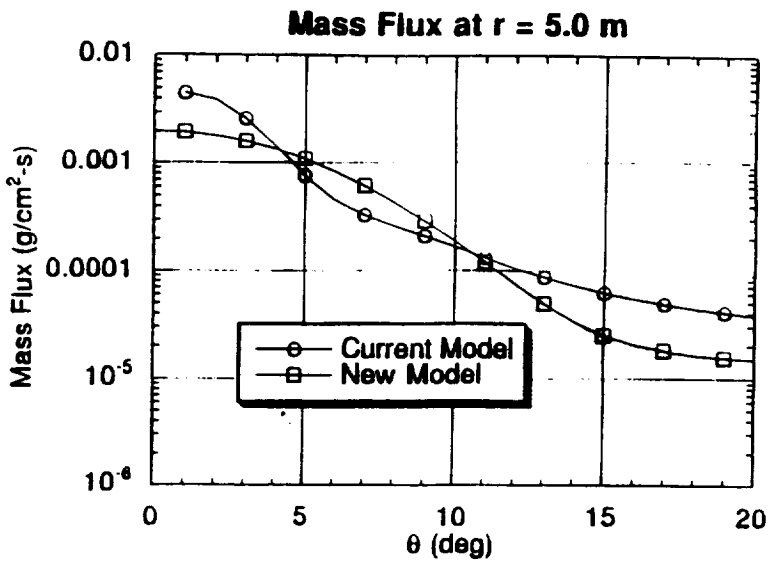Figure 8 : Comparison of Mass Flux at r=5m for the 1σ case and the Empirical Model

4-7

Figure 9 : Expanded View (0-20 degrees) of Figure 8
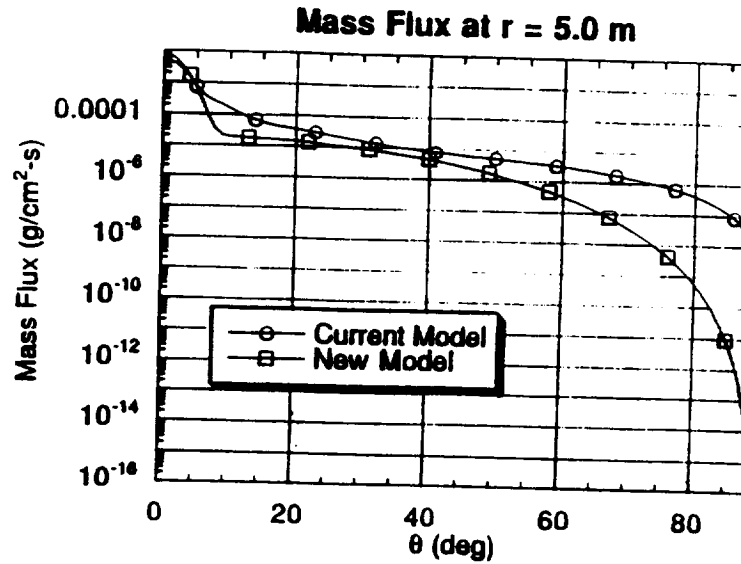
Figure 11 : Comparison of Mass Flux at r=5m for the 2σ case and the Empirical Model
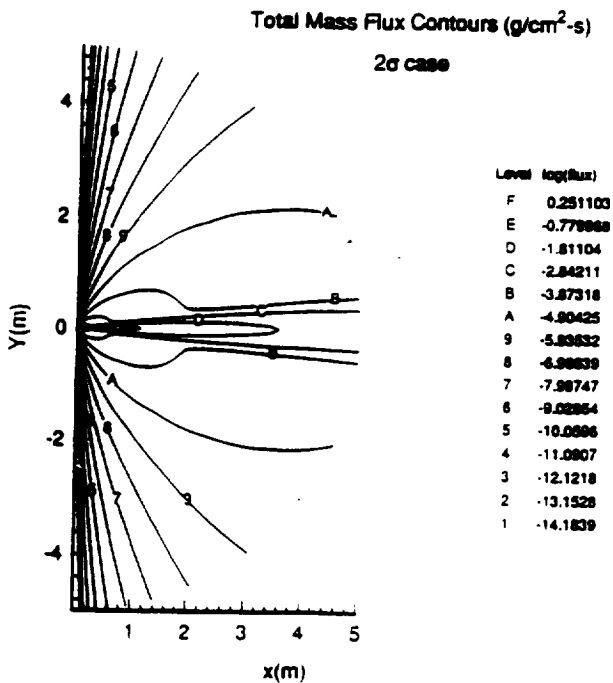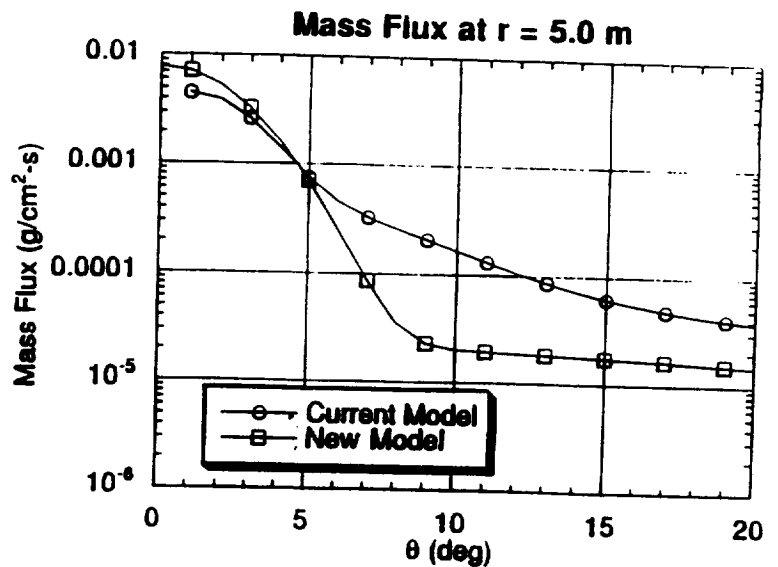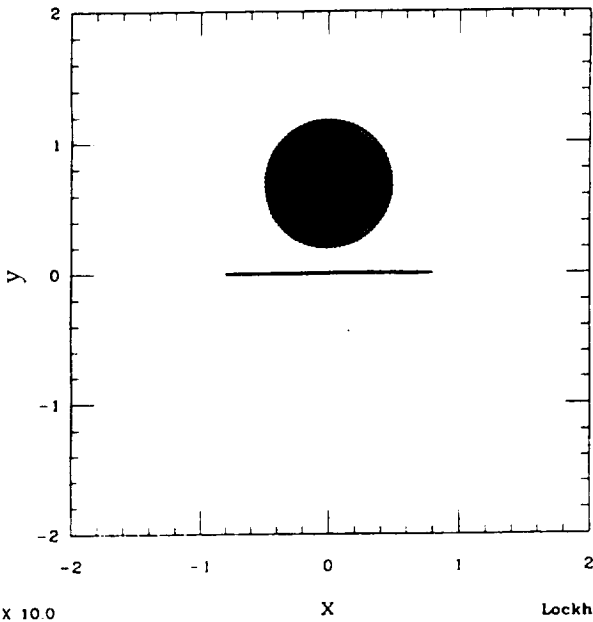

Figure 10 : Mass Flux Contours of the 2σ Case

Figure 12 : Expanded View (0-20 degrees) of Figure 11

Burt 1290 2d/t3d Time = 0.0944233 μs
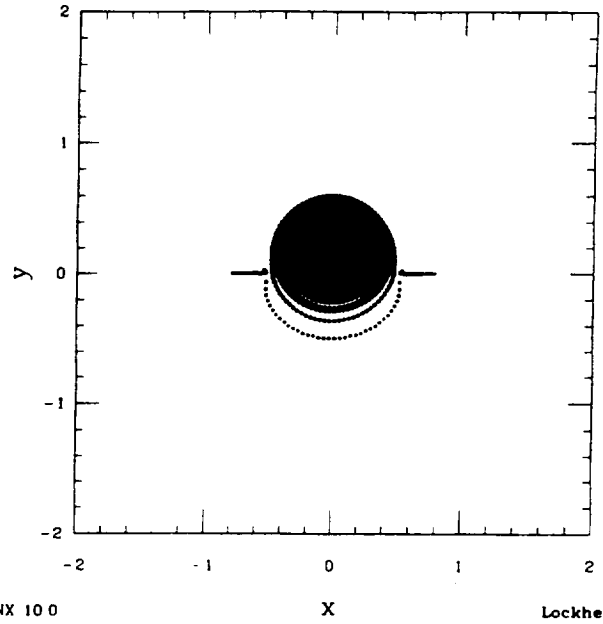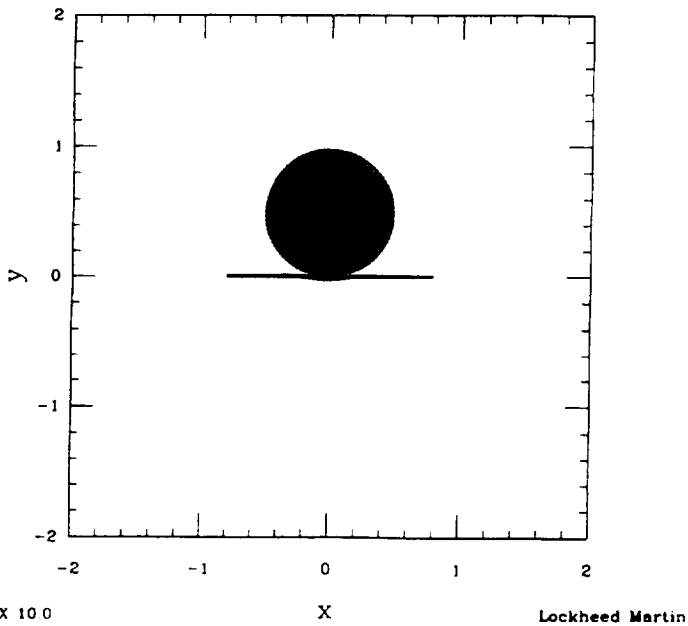
Burt 1290 2d/t3d Time = 0.938149 μs

Figure 13 : SPHINX Simulation of the Impact of
Aluminum Sphere on an Aluminum Plate
t = 0.0944233 μs

Figure 15 : SPHINX Simulation of the Impact of
Aluminum Sphere on an Aluminum Plate
t = 0.938149 μs

Burt 1290 2d/t3d Time = 0.550503 μs

Burt 1290 2d/t3d Time = 1.43971 μs

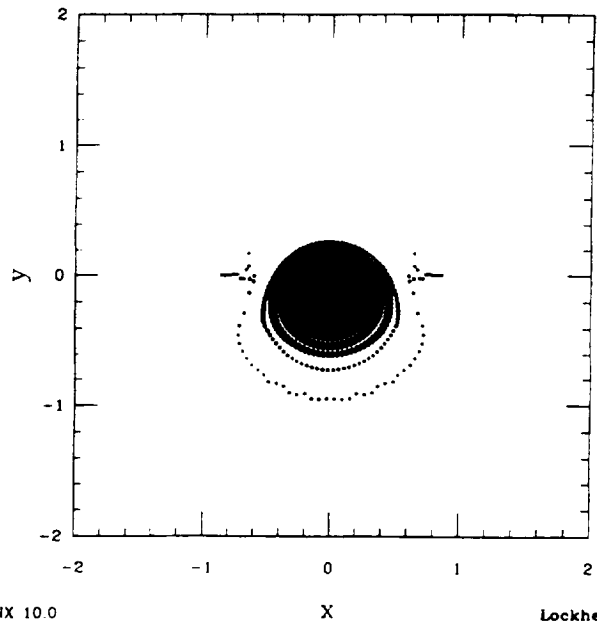Figure 14 : SPHINX Simulation of the Impact of
Aluminum Sphere on an Aluminum Plate
t = 0.550503 μs

Figure 16 : SPHINX Simulation of the Impact of
Aluminum Sphere on an Aluminum Plate
t = 1.43971 μs